JCMM Journal of Computers, Mechanical and Management
Journal homepage: www.jcmm.co.in
e-ISSN: 3009-075X
AN PUBLISHING

Volume 5 Issue 2
Article Number: 25388

Evaluation of Mechanical Properties of Graphene-Reinforced PETG Filaments Fabricated by FDM: Influence of Reinforcement and Process Parameters

Ram Kishore Shakya[1], Dharamvir Mangal[1], and Nagendra Kumar Maurya* [2]

[1]Mechanical Engineering Department, Gautam Buddha University, Greater Noida, India 201310
[2]Department of Mechanical Engineering, G.L. Bajaj Institute of Technology and Management, Greater Noida, India 201308

Abstract

In this study, graphene-reinforced polyethylene terephthalate glycol (PETG) composites are fabricated using the Fused Deposition Modeling (FDM) technique. The influence of process parameters, namely layer thickness, print speed, and nozzle temperature, on tensile and flexural strength is investigated. A Taguchi design of experiments is employed to optimize the process parameters, and regression models are developed to predict tensile strength and flexural strength. The optimum combination for tensile strength is identified as a layer thickness of 0.1 mm, print speed of 20 mm/s, and nozzle temperature of 230 °C, while the optimum combination for flexural strength is found at a layer thickness of 0.1 mm, print speed of 20 mm/s, and nozzle temperature of 235 °C. Microstructural characterization performed using Scanning Electron Microscopy (SEM) revealed uniform dispersion of graphene within the PETG matrix and strong interlayer bonding at optimized conditions. Fractography analysis conducted using Field Emission Scanning Electron Microscopy (FE-SEM) confirmed ductile fracture behavior with limited void formation. The developed regression models exhibited strong predictive accuracy, demonstrating their suitability for process optimization and the prediction of mechanical properties.

Keywords: FDM Process; Flexural Strength; Tensile Strength; Graphene Reinforcement

1. Introduction

Additive Manufacturing (AM) enables the direct fabrication of complex products from digital CAD models, facilitating customer-specific demand. Among AM techniques, Fused Deposition Modeling (FDM) has been widely used due to its low cost and material flexibility. FDM-manufactured components exhibit low mechanical properties due to weak interlayer bonding, process parameter variations, and different material compositions [1]. Improving the mechanical properties of FDM-printed components requires process optimization and material reinforcement. Polyethylene Terephthalate Glycol-modified (PETG) has proven to be a reliable FDM material, offering good transparency, ductility, balanced stiffness, and chemical resistance in comparison to ABS and PLA [2]. Dimensional stability and toughness are also comparatively better for PETG than ABS and PLA [3].

*Corresponding Author: Nagendra Kumar Maurya (nagendramnnit@gmail.com)
Received: 27 Dec 2025; Revised: 30 Jan 2026; Accepted: 28 Feb 2026; Published: 30 Apr 2026

DOI: 10.57159/jcmm.5.2.25388.

PETG is suitable for making functional components but is restricted for structural applications due to its moderate strength and limited stiffness. Reinforcement strategies enhance the mechanical performance of FDM-printed parts. Recent work has incorporated micro- and nanoparticle reinforcements, such as glass fibers, carbon fibers, carbon nanotubes (CNTs), and graphene nanoplatelets (GNPs), into the PETG matrix [4]. Incorporation of carbon fibers increases stiffness while reducing ductility, and incorporation of CNTs improves multifunctional characteristics, although their dispersion remains challenging [5]. Exceptional strength and surface area provided by graphene at low concentrations demonstrate significant potential to improve PETG composites. It was found that adding as little as 0.04 wt.% graphene enhances compressive strength, flexural strength, and tensile strength, indicating effective load transfer between the polymer matrix and graphene [6].

The mechanical properties of graphene-PETG (G-PETG) composite FDM-printed parts are found to be highly sensitive to process parameters, including printing speed, layer thickness, and nozzle temperature. Parameter variations influence porosity, crystallinity, and interlayer bonding [7]. Optimization has been conducted to support a comprehensive analysis of graphene-reinforced PETG and neat thermoplastics. Interactions between process conditions and reinforcement dispersion, such as the effect of temperature on graphene composition, are not well understood.

There is limited correlation among printing parameters, reinforcement dispersion, and filament compounding [7]. Few studies have examined interlayer toughness, fatigue, and fracture in G-PETG composites. Only a limited number of studies have investigated the effects of process parameters (e.g., layer height and nozzle temperature). There is a lack of understanding of optimal graphene loading (0.01–1.0 wt.%) due to inconsistent processing. Limited effort has been made toward integrating microstructural characterization (XRD, SEM, and micro-CT) with mechanical analysis [8].

The novelty of the present research lies in the combined influence of material extrusion process parameters on the tensile and flexural behavior of graphene-reinforced PETG filament. Unlike most existing studies that primarily focus on varying graphene content or reporting standalone mechanical improvements, this work emphasizes how critical printing parameters such as layer thickness, print speed, and nozzle temperature govern interlayer bonding and stress transfer at a fixed, practically viable graphene loading. The study provides new insights into the interaction between graphene's thermal and reinforcing characteristics and the thermal–mechanical history imposed during printing, thereby clarifying how process control can be leveraged to maximize mechanical performance.

2. Materials and Methods

2.1. Materials

In this research study, the research material, a graphene-reinforced PETG (polyethylene terephthalate glycol) filament, was procured from a commercial supplier (Graphenera Carbon Private Limited). The filament had a nominal diameter of 1.75 mm ± 0.05 mm. According to the supplier specifications, the graphene reinforcement consists of graphene nanoplatelets dispersed within the PETG matrix. The average lateral size of the platelets is in the micrometer range (5–10 µm), with an average thickness of 2–10 nm, corresponding to multilayer graphene. The graphene was used without additional surface functionalization and was incorporated into the filament during extrusion by the manufacturer. Graphene was incorporated into the PETG matrix by the manufacturer to improve the filament's strength, thermal conductivity, and interlayer adhesion, making it suitable for FDM printing applications.

Environmental control during printing was carefully maintained to account for PETG's moisture sensitivity. Before printing, the graphene-reinforced PETG filament was dried at 60 °C for 4 h in a convection dryer and subsequently stored in a sealed, desiccant-assisted container. Printing was performed under controlled laboratory conditions with a relative humidity of 40 ± 5% and an ambient temperature of 25 ± 2 °C. The filament was exposed to ambient air for less than 2 h during printing to minimize moisture uptake. These measures were adopted to ensure consistent extrusion quality, reduce porosity, and maintain interlayer bonding integrity. The selection of 1.0 wt.% graphene as a fixed reinforcement level was guided by the broader literature on graphene–polymer nanocomposites, which demonstrates that significant mechanical improvements can be achieved with low graphene loadings up to 1 wt.% due to graphene's high aspect ratio and interfacial reinforcement effect without severe agglomeration [9].

2.2. 3D Printing of Test Specimens

An FDM printer (Anycubic Kobra 3 Combo) was used to print all specimens. The printer's build volume was 250 × 250 × 260 mm. A Taguchi L9 orthogonal array was used for optimizing printing parameters and to study the influence of process parameters on mechanical properties. The Taguchi L9 experimental design is a statistical method used to minimize the number of experimental trials and optimize printing process parameters.

In the present study, the Taguchi optimization design employed three controllable printing parameters, namely print speed, layer thickness, and nozzle temperature, studied at three levels. In a full factorial design, 27 experimental runs would be required; the Taguchi L9 array reduces this to only 9. The Taguchi L9 array provides a balanced distribution of factor levels, allowing identification of the most significant parameters and their optimal settings with maximum reliability. The Taguchi method enhances design robustness by calculating the signal-to-noise (S/N) ratio, emphasizing parameter combinations that yield consistent performance and minimize external variations.

In this investigation, the L9 orthogonal array was used to systematically evaluate the effects of print speed, layer thickness, and nozzle temperature on the mechanical properties of graphene-reinforced PETG specimens printed via FDM, ensuring efficient experimentation and statistically meaningful conclusions. However, the L9 orthogonal array has inherent limitations, particularly in capturing higher-order interaction effects and in providing full predictive capability beyond the selected factor levels. The L9 design was chosen to efficiently screen the dominant process parameters with a minimal number of experiments while maintaining experimental feasibility. The results are interpreted primarily in terms of main effects.

The selected process parameters and their levels are listed in Table 1. The printing bed temperature was maintained at 80 °C. All specimens were fabricated using a rectilinear infill pattern with a nominal infill density of 100%, as defined by the slicing software. It is noted that in FDM processes, this setting corresponds to the maximum material deposition for the selected extrusion width and flow parameters and does not necessarily imply a completely void-free structure. An orientation of 0°/90°was used for all specimens, with the loading direction parallel to the deposited layers. A 0.4 mm nozzle was used with an extrusion width of 0.45 mm to ensure sufficient bead overlap and interlayer fusion. Each specimen was printed with 3 perimeters. The cooling fan speed was limited to 20% to avoid premature solidification and to promote polymer chain diffusion between layers, as recommended for PETG-based composites. Printing was carried out under ambient laboratory conditions (25 ± 2 °C) without an actively heated enclosure.

Specimens were prepared in accordance with ASTM D638 Type I (tensile) and ASTM D790 (flexural) standards [9]. After printing, all samples were conditioned at room temperature (23 ± 2 °C) for 24 h before testing. Table 2 shows the Taguchi orthogonal array L9. Figure 1 shows the 3D CAD models and 3D-printed test specimens for tensile and flexural testing. Three samples were printed for each experimental run, and their average value was used for data analysis.

Table 1: Process parameters and their levels

Process Parameters	**Level 1**	**Level 2**	**Level 3**
Layer Thickness (mm)	0.1	0.15	0.2
Print Speed (mm/s)	20	40	60
Nozzle Temperature (°C)	230	235	240

Table 2: Experimental plan (Taguchi L9 orthogonal array)

Run	**Layer Thickness**	**Print Speed**	**Nozzle Temp**
1	1	1	1
2	1	2	2
3	1	3	3
4	2	1	2
5	2	2	3
6	2	3	1
7	3	1	3
8	3	2	1
9	3	3	2

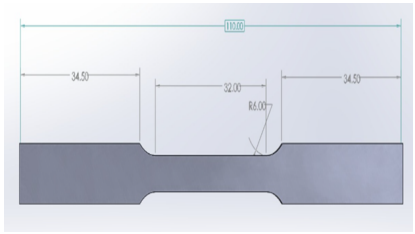

(a) 3D CAD model of the tensile test specimen

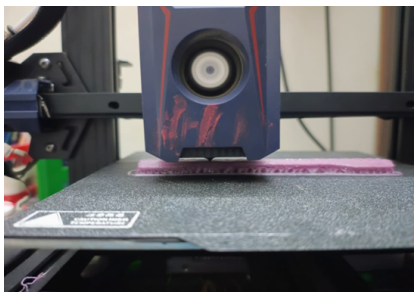

(b) 3D-printed tensile test specimen

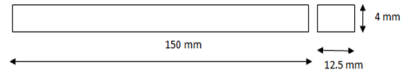

(c) Dimensions of flexural test specimen

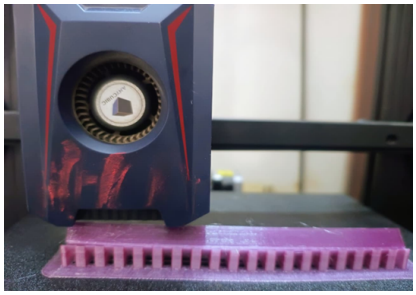

(d) 3D-printed bending test specimen

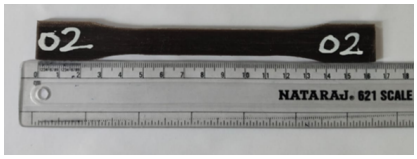

(e) Printed tensile test specimen showing scale

(f) Printed bending test specimen showing scale

Figure 1: Test specimens used in the study

2.3. Evaluation of Tensile Strength

Dog-bone specimens of graphene-reinforced PETG were 3D-printed to ASTM D638 Type I dimensions, conditioned at 25 ± 2 °C and 50 ± 5% RH for 24 h, and tested on an Instron universal testing machine (System ID 3382AB1533) calibrated on 18-03-2024 [10]. The frame was fitted with a 100 kN load cell. Tests were performed at a crosshead speed of 0.5 mm min^{-1} (rigid plastics per ASTM D638) and a gauge length of 32 mm; an extensometer was used to measure deformation. Force–displacement data were converted to engineering stress–strain using the initial cross-sectional area (A_0) of the fabricated test specimen and original gauge length (L_0). Ultimate tensile strength (σ_{UTS}) was computed as:

$$\sigma_{\text{UTS}} = \frac{F_{\text{max}}}{A_0} \tag{1}$$

The dimensions of the fabricated and CAD specimens, including length, width, and thickness, are reported in Table 3. For each experimental run, 3 replicates were tested; results are reported as mean ± SD. Figure 2 shows the fabricated tensile test specimens, tensile testing of 3D-printed specimens, and fractured tensile test specimens.

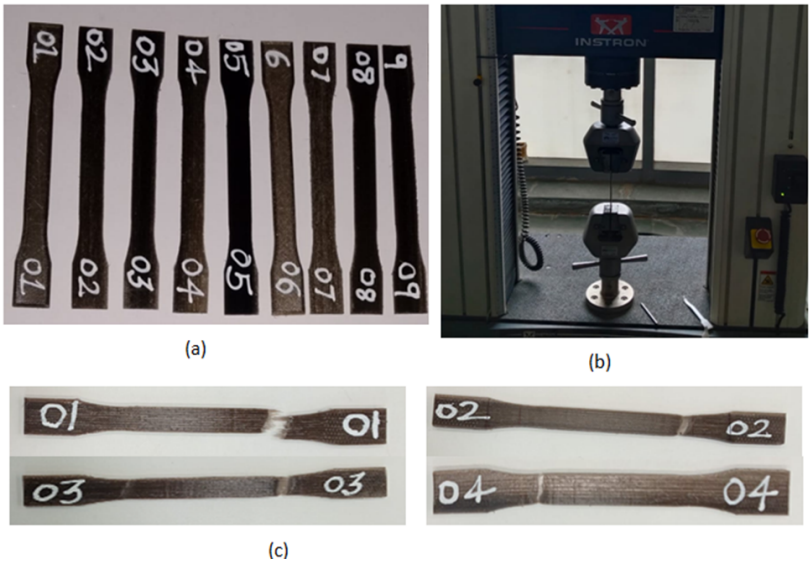

Figure 2: (a) Fabricated tensile test specimens, (b) Tensile testing of 3D-printed specimens, (c) Fractured tensile test specimen.

2.4. Evaluation of Flexural Strength

The flexural strength of the 3D-printed PETG/graphene composite specimens was evaluated using the same universal testing machine (UTM) (System ID 3382AB1533) calibrated on 18-03-2024. The test environment for the flexural test was the same as the tensile test: 25 ± 2 °C and 50 ± 5% RH. The test was conducted following the ASTM D790 standard for polymeric materials [11, 12]. A three-point bending fixture was mounted on the UTM, consisting of two support rollers and a centrally applied loading nose. The specimens were printed and surface-finished to remove burrs formed during printing. The dimensions of the test specimen were 150 mm × 12.7 mm × 4 mm. The span length between supports was maintained at 64 mm, corresponding to a span-to-depth ratio of 16:1. The crosshead speed was set to 2 mm/min, ensuring quasi-static loading conditions.

During testing, the load and deflection were continuously recorded using the machine's integrated data acquisition system. The flexural strength was determined from the load-deflection curves. All tests were conducted at ambient laboratory conditions (temperature 25 ± 2 °C and relative humidity 50 ± 5%). Three specimens were tested for each set of process parameters to ensure repeatability and to minimize experimental uncertainty [13, 14]. Table 3 shows the average values of measured tensile strength and flexural strength of printed samples. Figure 3 shows the flexural test setup.

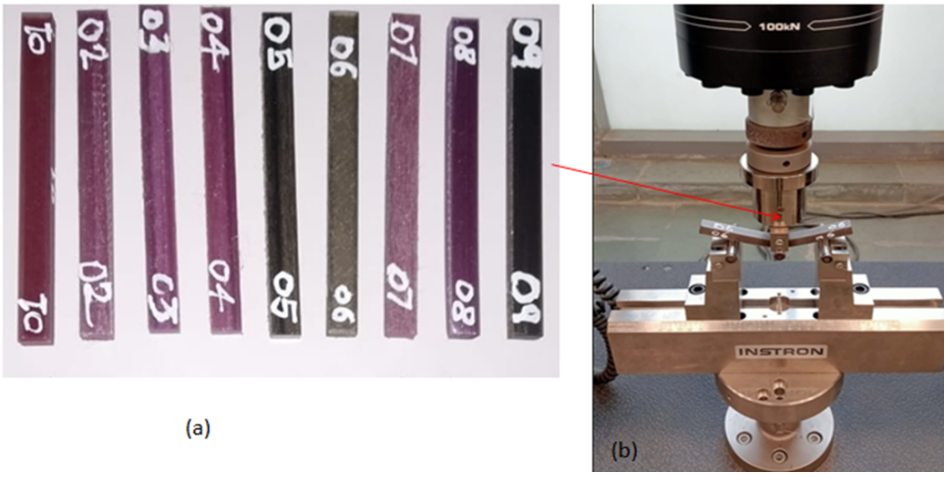

Figure 3: (a) Flexural test specimen, (b) Flexural strength testing on Instron machine.

Table 3: Average tensile strength and flexural strength of printed samples

Run	Layer (mm)	Speed (mm/s)	Temp (°C)	Actual Thick. (mm)	Tensile Strength (MPa)	Flexural Strength (MPa)
1	0.1	20	230	4.192	55.12 ± 1.4	80.91 ± 3.8
2	0.1	40	235	4.056	52.23 ± 1.2	78.13 ± 2.9
3	0.1	60	240	4.064	50.34 ± 0.98	75.89 ± 3.9
4	0.15	20	235	4.004	53.56 ± 1.1	77.21 ± 1.8
5	0.15	40	240	4.02	51.25 ± 1.3	74.35 ± 2.4
6	0.15	60	230	4.232	50.87 ± 0.99	73.46 ± 1.8
7	0.2	20	240	4.1	48.92 ± 1.8	72.78 ± 1.9
8	0.2	40	230	4.168	47.14 ± 1.5	70.32 ± 2.2
9	0.2	60	235	4.084	46.23 ± 1.5	69.37 ± 2.6

3. Results and Discussion

3.1. Development of Regression Models for Tensile Strength and Flexural Strength

To establish the relationship between the FDM process parameters and the mechanical performance of graphene-reinforced PETG composites, linear regression models were developed for tensile and flexural strengths as functions of the coded values of layer thickness, print speed, and nozzle temperature.

The statistical adequacy of the developed models was evaluated based on the coefficient of determination (R^2), adjusted R^2, predicted R^2, and standard deviation (S) values, as obtained from the model summary and ANOVA results [15].

The tensile strength model exhibited an R^2 value of 0.873; adjusted R^2 (0.7968) and predicted R^2 (0.623) values suggest a reasonably good fit with moderate predictive capability. The standard deviation ($S = 1.29771$) indicates an acceptable level of residual error between experimental and predicted values. However, this regression analysis was primarily presented as a trend-based tool to identify the relative influence of process parameters and to support comparative optimization within the studied design space, rather than as a strong predictive model.

The ANOVA results presented in Table 4 indicate that the overall regression model is statistically significant ($F = 11.46$, $p = 0.011$), confirming that process parameters influence tensile strength significantly. Nozzle temperature ($F = 0.68$, $p = 0.44$) had an insignificant effect, while layer thickness ($F = 23.47$, $p = 0.005$) was found to be the most significant factor, followed by print speed ($F = 10.22$, $p = 0.024$). The negative influence of print speed and higher layer thickness is attributed to increased interlayer voids and reduced interfacial bonding, which deteriorate load transfer efficiency within the printing system. Equation 2 shows the developed model for tensile strength.

In the case of the flexural strength model, significantly higher goodness of fit was observed, with $R^2 = 0.9793$, adjusted $R^2 = 0.9669$, and predicted $R^2 = 0.928$, reflecting good agreement between predicted responses and experimental responses. The relatively low standard deviation ($S = 0.6667$) indicates minimal deviation between model-predicted values and measured values. ANOVA analysis (Table 5) confirms that the models are statistically significant ($F = 79.00$, $p = 0.000$).

Similar to tensile strength, layer thickness ($F = 181.50$, $p = 0.000$) emerged as the most dominant factor affecting flexural strength, followed by print speed ($F = 54.00$, $p = 0.001$), while nozzle temperature ($F = 1.50$, $p = 0.275$) remained statistically insignificant. The high sensitivity of flexural strength to layer thickness is attributed to its direct influence on interlayer adhesion and on structural continuity across the neutral axis during bending. Thinner layers promote better fusion between successive filaments, thereby enhancing load-carrying capacity under bending conditions. Equation 3 shows the developed model for flexural strength. The S/N ratio can be calculated from Equation 4.

$$\text{Tensile Strength (MPa)} = 60.02 - 2.567 \times \text{Layer Thickness} - 1.693 \times \text{Print Speed} - 0.437 \times \text{Nozzle Temp} \quad (2)$$

$$\text{Flexural Strength (MPa)} = 86.222 - 3.667 \times \text{Layer Thickness} - 2.000 \times \text{Print Speed} - 0.333 \times \text{Nozzle Temp} \quad (3)$$

For the Taguchi Signal-to-Noise (S/N) ratio with the "Larger-is-Better" quality characteristic, the calculation uses:

$$\text{S/N} = -10 \log \left(\frac{1}{n} \sum_{i=1}^{n} \frac{1}{y_i^2} \right) \quad (4)$$

where y_i is the observed response value in the ith trial and n is the number of observations (replications).

Table 4: Analysis of variance for tensile strength

Source	**DF**	**Adj SS**	**Adj MS**	**F-Value**	**P-Value**
Regression	3	57.875	19.292	11.46	0.011
Layer Thickness (mm)	1	39.527	39.527	23.47	0.005
Print Speed (mm/s)	1	17.204	17.204	10.22	0.024
Nozzle Temp (°C)	1	1.144	1.144	0.68	0.447
Error	5	8.420	1.684		
Total	8	66.295			

Table 5: Analysis of variance for flexural strength

Source	**DF**	**Adj SS**	**Adj MS**	**F-Value**	**P-Value**
Regression	3	105.333	35.1111	79.00	0.000
Layer Thickness (mm)	1	80.667	80.6667	181.50	0.000
Print Speed (mm/s)	1	24.000	24.0000	54.00	0.001
Nozzle Temp (°C)	1	0.667	0.6667	1.50	0.275
Error	5	2.222	0.4444		
Total	8	107.556			

3.2. Effect of Process Variables on Tensile Strength

Main effects plots, surface plots, a Pareto chart, and residual analysis were used to examine the impact of the main process parameters on the tensile strength of the 3D-printed samples, namely layer thickness, print speed, and nozzle temperature. Table 6 presents tensile strength S/N ratios.

Figure 4(a) indicates that the main effects plot reveals that layer thickness has a significant impact on tensile strength. The results revealed that specimens printed with a smaller layer thickness exhibited superior tensile strength than those printed with a larger layer thickness. This improvement is primarily due to enhanced heat transfer and interlayer bonding during the material extrusion process. A reduced layer thickness increases the number of deposited layers for a given part height, resulting in repeated thermal exposure of previously deposited layers. This promotes improved thermal diffusion and interdiffusion of polymer chains across adjacent layers, leading to stronger interfacial bonding.

From a porosity perspective, thinner layers allow more uniform material flow and better filling of inter-raster gaps, thereby reducing void formation and interlayer defects. In contrast, a larger layer thickness limits adequate heat penetration into the underlying layer, resulting in insufficient fusion and higher porosity, which act as stress concentration sites and reduce tensile strength. The presence of graphene further influences this behavior. Due to its high thermal conductivity, graphene facilitates localized heat dissipation and improves thermal homogeneity within the deposited filament. At a smaller layer thickness, this effect becomes more pronounced, as the enhanced heat distribution supports improved melting and wetting between layers, strengthening the graphene–PETG interface. Additionally, well-dispersed graphene restricts polymer chain mobility and contributes to effective load transfer, thereby delaying crack initiation and propagation under tensile loading.

Tensile strength is also highly influenced by print speed. Tensile strength decreases as printing speed increases. Increased speed reduces the time available for adequate heat transfer between the extruded filament and the existing layer, thereby decreasing interfacial adhesion. Conversely, low print speeds enhance layer melting and diffusion, leading to improved bonding and tensile strength. When nozzle temperature is increased moderately, tensile strength initially increases; however, excessive temperatures may cause material degradation or over-melting, thereby weakening structural integrity. Therefore, an optimal temperature interval is key to achieving the best mechanical performance.

Figure 4(b) indicates that surface plots show that a combination of low layer thickness and medium print speed achieves optimum tensile strength. The interaction effects appear insignificant, indicating that tensile strength is largely controlled by the main effects of the process parameters rather than their interactions. The Pareto Chart of Standardized Effects (Figure 4(c)) also confirms that layer thickness (A) was the most influential variable on tensile strength, followed by print speed (B). The effect of nozzle temperature (C) is comparatively smaller but falls under the significance level ($\alpha = 0.05$).

As demonstrated in Figure 4(d), results of the Residual Plots (Normal Probability, Histogram, and Versus Fits) confirm the suitability of the regression model. Normal distribution is confirmed because the normal probability plot shows that the residuals are nearly distributed along a straight line. The residuals show no systematic trend, and the order plots show no systematic pattern, indicating that the model is reliable and free of bias.

Figure 4(e) shows the interaction plot for tensile strength, revealing notable interaction effects among layer thickness, print speed, and nozzle temperature. The interaction between layer thickness and print speed shows non-parallel trends, indicating that the influence of print speed on tensile strength depends on the selected layer thickness. At lower layer thickness, tensile strength decreases more sharply with increasing print speed, whereas at higher layer thickness, the variation is comparatively moderate, suggesting improved process stability. A similar interaction is observed between layer thickness and nozzle temperature: tensile strength decreases with increasing nozzle temperature at lower layer thicknesses but exhibits a less pronounced change at higher thicknesses, indicating reduced thermal sensitivity. The interaction between print speed and nozzle temperature is stronger, as evidenced by the intersecting lines, suggesting that the combined effect of these parameters significantly governs interlayer bonding and material consolidation.

Table 6: Signal-to-noise ratios for tensile strength

Level	**Layer Thickness (mm)**	**Print Speed (mm/s)**	**Nozzle Temp (°C)**
1	34.41	34.40	34.14
2	34.30	34.01	34.08
3	33.52	33.82	34.01
Delta	0.89	0.58	0.13
Rank	1	2	3

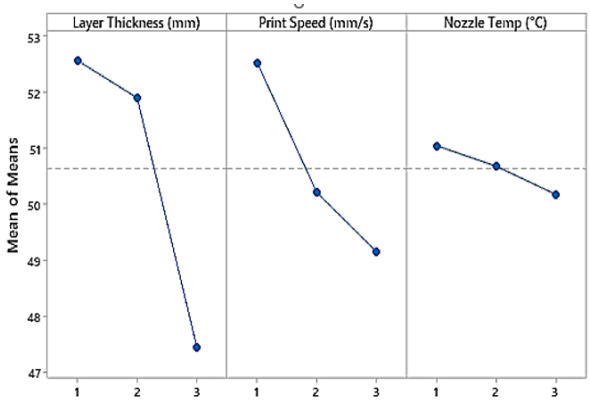

(a) Main effect plot for tensile strength

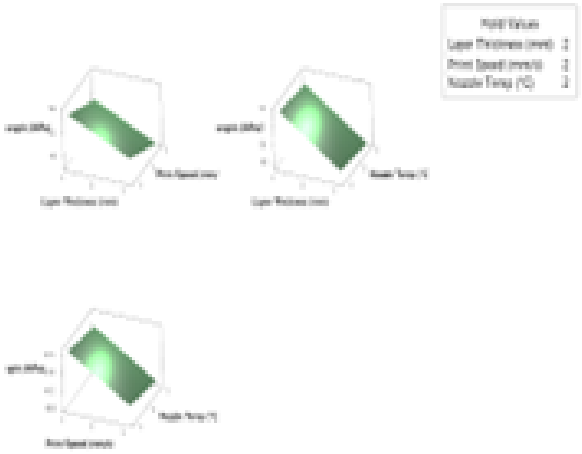

(b) Surface plot of process variables

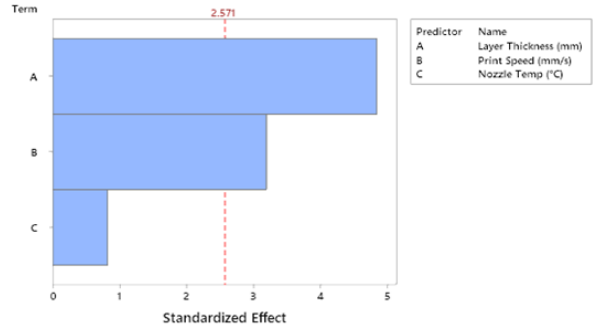

(c) Pareto chart

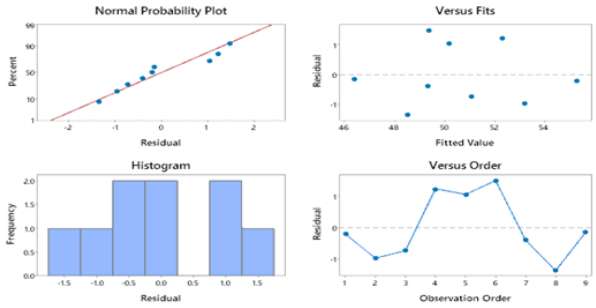

(d) Residual plot for tensile strength

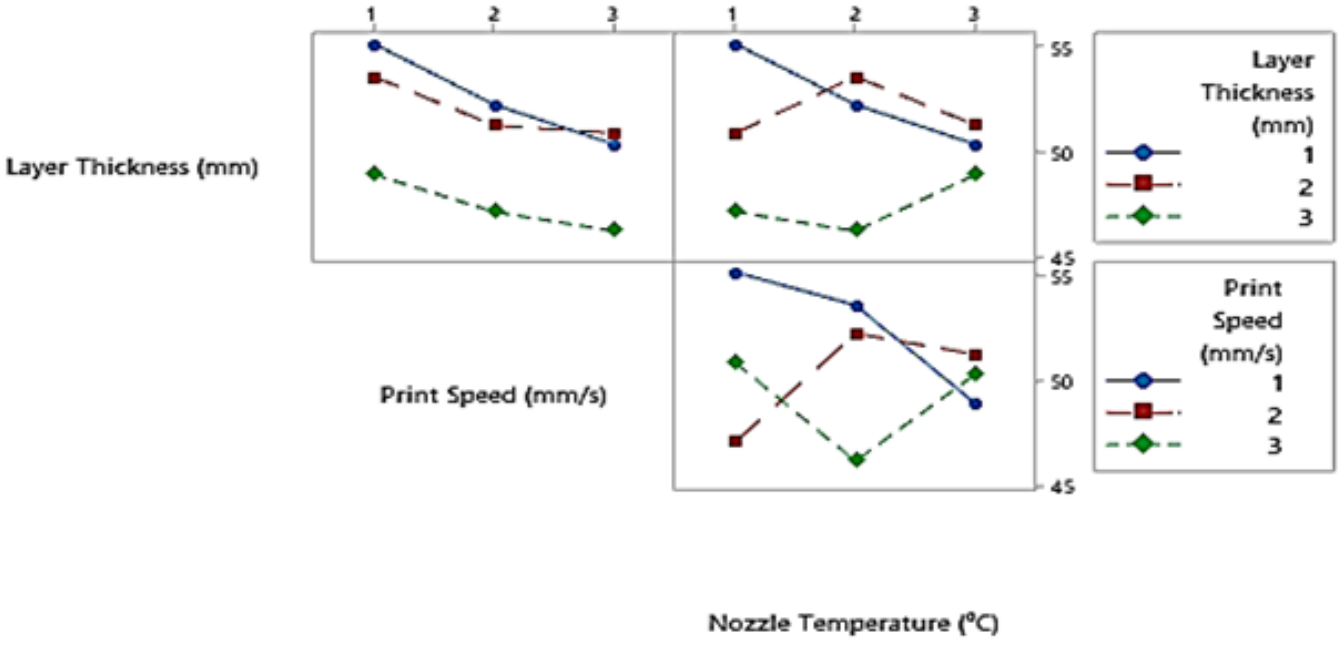

(e) Interaction plot

Figure 4: Tensile strength analysis plots

The stress–strain curves of samples are illustrated in Figure 5. Analysis of the stress–strain curves shows that the maximum strain at break lies in the range of approximately 4–12%, depending on the processing condition. These elongation-at-break values, together with the presence of dimples and plastic deformation features observed in the FE-SEM fractographs, substantiate the ductile fracture behavior.

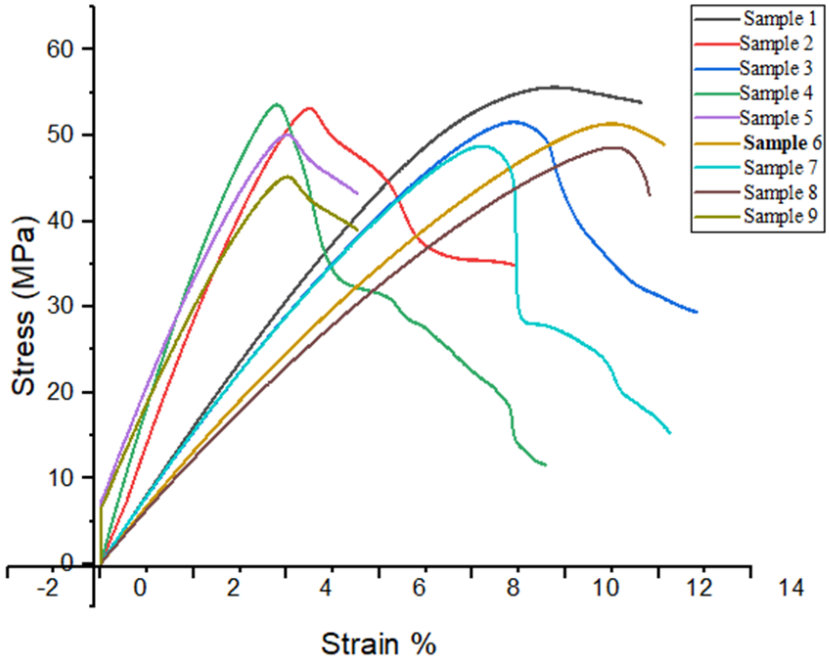

Figure 5: Stress versus strain curves of fabricated samples.

3.3. Effect of Process Parameters on Flexural Strength

The main effects plot of S/N ratios and the Pareto chart of standardized effects were used to examine the effect of FDM process parameters, namely layer thickness, print speed, and nozzle temperature, on the flexural strength of graphene-reinforced PETG composite. The Main Effects Plot in Figure 6(a) represents the S/N ratios where the "larger is better" criterion is used. Results showed that flexural strength is most affected by layer thickness. The S/N ratio (Table 7) reduces significantly with an increase in layer thickness, which implies that smaller layer thickness results in greater flexural strength. This is because thinner layer thicknesses lead to stronger interlayer bonding and lower void content, enabling more effective load transfer between layers. Thicker layers, conversely, exacerbate poor interfacial bonding and an uneven distribution of graphene particles, which act as stress concentrators and reduce bending resistance. Print speed also plays a significant role in flexural performance. Higher print speed yields a lower S/N ratio, indicating that slower print speed results in higher flexural strength. This is attributed to adequate residence time for heat transfer and diffusion among deposited filaments, which facilitates high interlayer adhesion. At higher speeds, degraded bonding between adjacent layers and irregularities in graphene dispersion degrade mechanical properties. The nozzle temperature has a comparatively minor impact on flexural strength in comparison to layer thickness and print speed. As nozzle temperature is moderately increased, the rate of material flow and the dispersion of graphene in the PETG composite improve, thereby increasing bonding strength. Nevertheless, large increments can degrade the polymer matrix or induce thermal stress, thereby decreasing the overall flexural strength by a small margin.

The Pareto Chart of Figure 6(b) in Standardized Effects confirms that the most dominant parameter affecting flexural strength is layer thickness (A), followed by print speed (B), and lastly nozzle temperature (C), which is below the significance level ($\alpha = 0.05$). Figure 6(c) represents the surface plot for flexural strength, and Figure 6(d) represents the residual plot for flexural strength. Figure 6(e) shows the interaction plot for flexural strength, indicating pronounced interaction effects among layer thickness, print speed, and nozzle temperature. The interaction between layer thickness and print speed shows nearly parallel downward-sloping trends, suggesting that flexural strength consistently decreases with increasing print speed across all layer thicknesses, while thinner layers yield higher strength due to improved interlayer bonding. The interaction between layer thickness and nozzle temperature shows mild non-parallel behavior, indicating that nozzle temperature has a stronger influence at lower layer thickness, where an optimal temperature enhances material fusion and flexural performance. In contrast, the interaction between print speed and nozzle temperature is strong, as evidenced by intersecting lines, revealing that the effect of nozzle temperature on flexural strength is highly dependent on print speed. Moderate nozzle temperatures combined with intermediate print speeds yield the highest flexural strength, whereas higher speeds or temperatures reduce bonding efficiency. These findings are important because interlayer bonding, heat transfer, and uniformity of graphene distribution are crucial elements that determine the flexural performance of printed composites. The best flexural strength is achieved by combining a minimum layer thickness, a low print speed, and an optimal nozzle temperature that enhances polymer chain diffusion and evenly distributes the graphene reinforcement. Table 8 shows a comparative study with the present work.

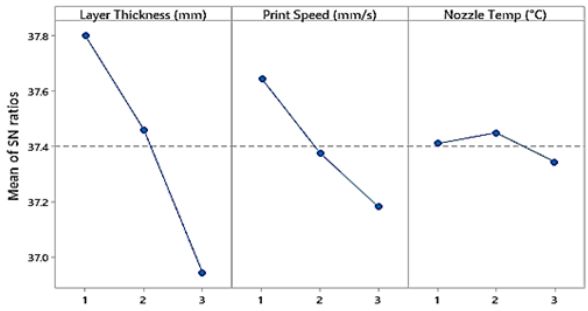

(a) Main effect plot for flexural strength

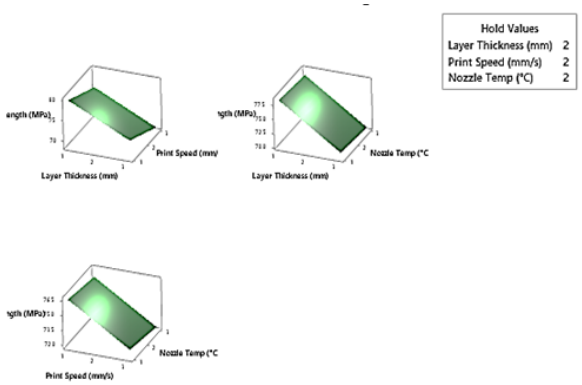

(b) Surface plot of process variables

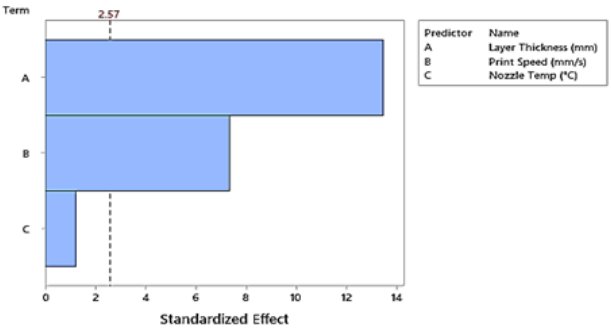

(c) Pareto chart

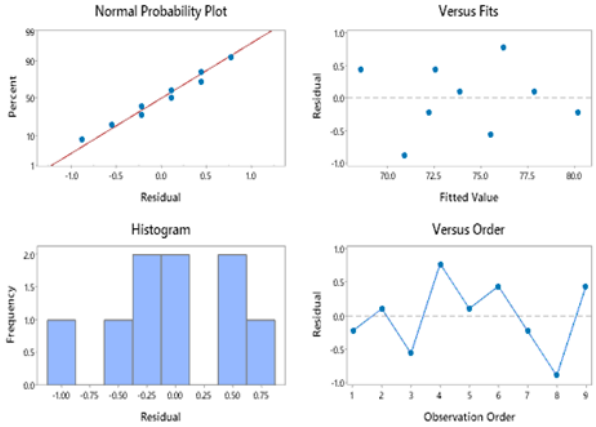

(d) Residual plot for flexural strength

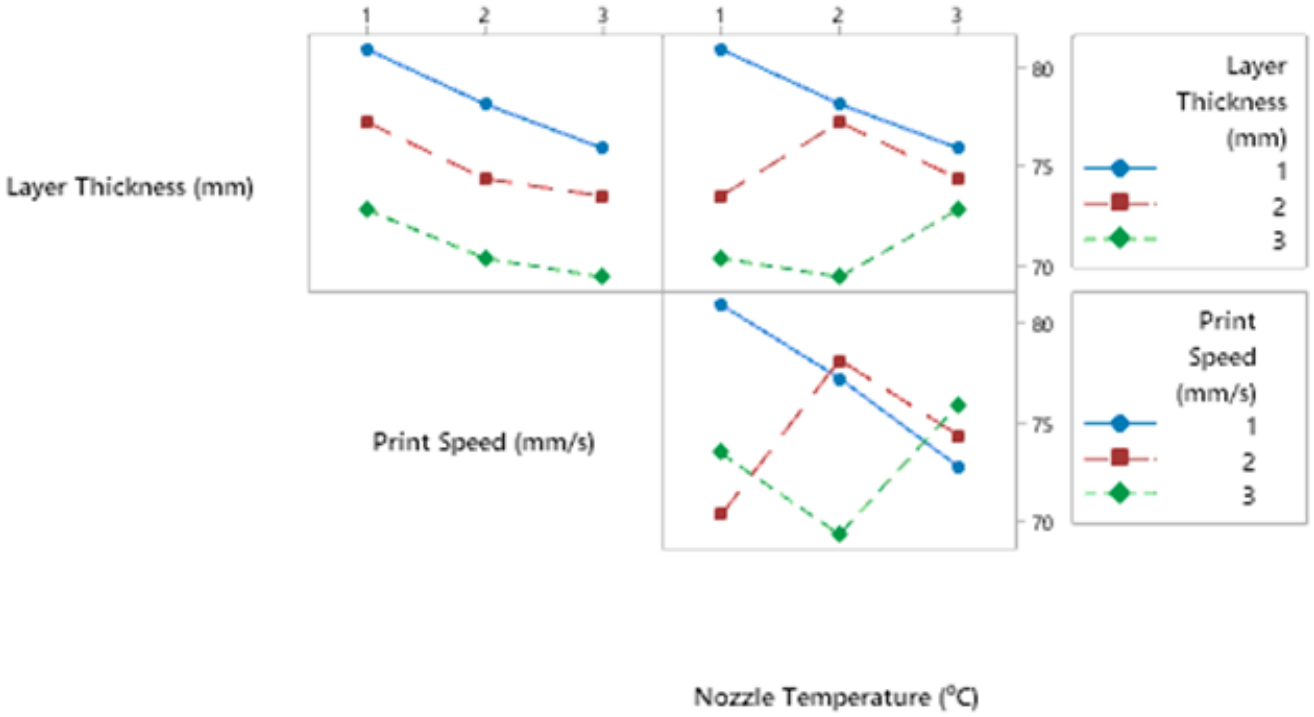

(e) Interaction plot

Figure 6: Flexural strength analysis plots

Table 7: Signal-to-noise ratios for flexural strength

Level	**Layer Thickness (mm)**	**Print Speed (mm/s)**	**Nozzle Temp (°C)**
1	37.80	37.65	37.41
2	37.46	37.38	37.45
3	36.94	37.18	37.34
Delta	0.86	0.46	0.11
Rank	1	2	3

Table 8: Comparative study with present work

Material	**Process Parameters**	**Mechanical Properties**	**Optimum Parameters**	**Ref.**
Gr 1 wt.% PETG	Layer thickness, Nozzle temp, Printing speed	UTS 55.32 MPa, Flexural 79.89 MPa	Layer 0.1 mm, speed 20 mm/s, temp 230 °C	Present
G-PETG (AHP)	Layer height, print speed, raster angle	UTS 49.1 MPa, E 735.6 MPa	Layer 0.20 mm, 40 mm/s, 0°raster	[16]
G-PETG (FAHP-TOPSIS)	Infill density, layer height, print speed, temp	UTS 56.16 MPa	65% infill, 0.20 mm, 50 mm/s, 240 °C	[17]
PETG with Graphene	Not specified	Tensile 50 MPa, Flexural 95 MPa	—	[18]
PETG	Layer height, raster angle, build orientation	Tensile 48 MPa, Flexural 68 MPa	Layer 0.20 mm, raster 0°, flat	[19]

3.4. Microstructural Analysis

The SEM micrograph of the graphene-reinforced PETG specimen fabricated using the FDM process (Figure 7) reveals the surface morphology and interfacial features at different magnifications (100×, 150×, 500×, and 997×). The surface appears smooth, with minor undulations, indicating good layer adhesion and consistent material deposition during printing. Some discrete particle agglomerates are observed; they are attributed to localized clustering of graphene nanoparticles within the PETG matrix. These agglomerates suggest partial dispersion of graphene, a common phenomenon due to strong van der Waals interactions between graphene sheets.

The absence of major voids at the layer interfaces indicates satisfactory fusion between successive printed layers, demonstrating the effectiveness of the selected process parameters. Regions in which graphene is richly embedded within the polymer matrix appear as bright contrast areas, where load transfer capability is enhanced, improving both flexural and tensile strength. Minor thermal inconsistencies during extrusion are indicated in the tilted traces. The SEM analysis shows a uniform and well-consolidated printed structure along with a moderately homogeneous graphene distribution, which validates the suitability of FDM technology for fabricating graphene-reinforced composites.

3.5. Fractographic Analysis

A SEM micrograph of a fractured graphene-reinforced PETG composite sample (Figure 8) was obtained after tensile testing, providing valuable insights into the interlayer bonding characteristics and fracture behavior of FDM-printed structures. Layer-by-layer morphology is observed at magnifications of 51×, 250×, and 497× of different layers of the FDM-printed specimen. Improper coalescence among extruded layers is evident from the semi-fused filament morphology, indicating that interlayer diffusion of molten polymer did not occur fully; this is attributed to thermal gradients and cooling rates during deposition.

Analysis shows that the fractured surface exhibits both brittle and ductile failure characteristics. Many regions display stretched, elongated filaments and fibrillated zones, suggesting localized plastic deformation prior to fracture, whereas other regions exhibit flat, smooth facets indicative of brittle fracture. The presence of inter-bead gaps and voids suggests that interlayer adhesion was the weakest link in the sample's failure. This feature is characteristic of FDM-printed composites, where anisotropy and insufficient fusion are the dominant failure mechanisms.

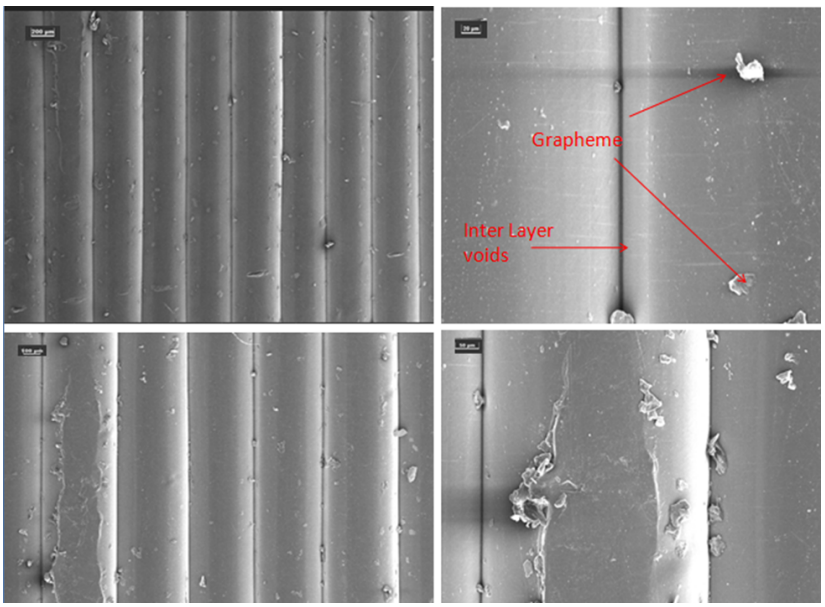

Figure 7: SEM micrograph of 3D-printed graphene/PETG composite exhibiting uniform deposition and minor graphene agglomeration.

Uniform graphene dispersion and filament fusion-dominated bonding are correlated with enhanced load transfer and higher strength. Furthermore, graphene agglomeration and brittle fracture features contribute to localized stiffness mismatch, crack propagation, and strength degradation. The reinforced graphene nanoparticles embedded in the PETG matrix likely enhance load transfer efficiency and restrict polymer chain mobility, thereby increasing strength and stiffness. The aggregation of graphene in particular areas may have acted as local stress concentration points, initiating microcracks under tensile loading. The overall morphology suggests that while graphene reinforcement improved interlayer cohesion and mechanical integrity, optimizing process parameters, such as nozzle temperature and print speed, is essential to enhance interlayer diffusion and minimize void formation.

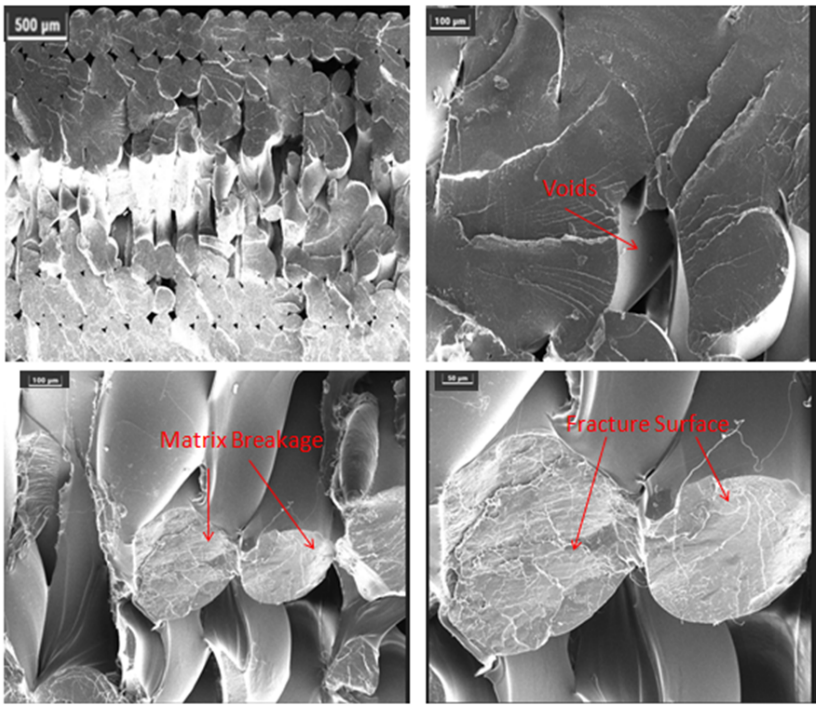

Figure 8: SEM micrograph of fracture surface at different magnifications.

4. Conclusions

The present research comprehensively investigated the effects of key FDM process parameters — layer thickness, print speed, and nozzle temperature — on the mechanical performance of graphene-reinforced PETG composites. Experimental results revealed that the optimum combination of process parameters for achieving maximum tensile strength (55.32 MPa) was a layer thickness of 0.1 mm, print speed of 20 mm/s, and nozzle temperature of 230 °C, whereas the optimum condition for flexural strength (79.89 MPa) was a layer thickness of 0.1 mm, print speed of 20 mm/s, and nozzle temperature of 235 °C. The developed regression models for both responses exhibited good predictive accuracy, confirming their reliability for process optimization. Graphene exhibits a generally homogeneous distribution with localized agglomeration, which is consistent with the SEM observations. Fractography analysis (FE-SEM) shows intact fracture surfaces with minimal voids, indicating enhanced interfacial adhesion and efficient stress transfer between the polymer matrix and the graphene reinforcement.

Author Contributions

Ram Kishore Shakya: Conceptualization, Methodology, Investigation, Data curation, Writing: original draft; **Dharamvir Mangal**: Supervision, Writing: review and editing; **Nagendra Kumar Maurya**: Supervision, Validation, Writing: review and editing.

Declaration of Competing Interests

The authors declare that they have no known competing financial interests or personal relationships that could have appeared to influence the work reported in this paper.

Data Availability Statement

The data that support the findings of this study are available from the corresponding author upon reasonable request.

Use of Generative AI

AI-assisted tools were used solely for language and grammar improvement. The authors retain full responsibility for the scientific content and conclusions.

Acknowledgment

The authors would like to acknowledge Gautam Buddha University and G.L. Bajaj Institute of Technology and Management for providing the necessary facilities and support for conducting this research.

Funding Declaration

No funding or financial support was received for this research work.

Ethics Approval and Consent

This study does not involve human participants, animals, or sensitive personal data. No ethics approval was required.

References

[1] K. S. Patel, D. B. Shah, S. J. Joshi, F. K. Aldawood, and M. Kchaou, "Effect of process parameters on the mechanical performance of fdm printed carbon fiber reinforced petg," *Journal of Materials Research and Technology*, vol. 30, pp. 8006–8018, 2024.

[2] M. A. Kumar, M. S. Khan, and S. B. Mishra, "Effect of machine parameters on strength and hardness of fdm printed carbon fiber reinforced petg thermoplastics," *Materials Today: Proceedings*, vol. 27, pp. 975–983, 2020.

[3] S. Valvez, A. P. Silva, and P. N. Reis, "Optimization of printing parameters to maximize the mechanical properties of 3d-printed petg-based parts," *Polymers*, vol. 14, no. 13, p. 2564, 2022.

[4] K. S. Kumar, R. Soundararajan, G. Shanthosh, P. Saravanakumar, and M. Ratteesh, "Augmenting effect of infill density and annealing on mechanical properties of petg and cfpetg composites fabricated by fdm," *Materials Today: Proceedings*, vol. 45, pp. 2186–2191, 2021.

[5] M. Batista, J. M. Lagomazzini, M. R.-P. na, and J. M. Vazquez-Martinez, "Mechanical and tribological performance of carbon fiber-reinforced petg for fff applications," *Applied Sciences*, vol. 13, no. 23, p. 12701, 2023.

[6] V. Mahesh, A. S. Joseph, V. Mahesh, D. Harursampath, and C. Vn, "Investigation on the mechanical properties of additively manufactured petg composites reinforced with ommt nanoclay and carbon fibers," *Polymer Composites*, vol. 42, no. 5, pp. 2380–2395, 2021.

[7] E. García, P. J. N. nez, M. A. Caminero, J. M. Chacón, and S. Kamarthi, "Effects of carbon fibre reinforcement on the geometric properties of petg-based filament using fff additive manufacturing," *Composites Part B: Engineering*, vol. 235, p. 109766, 2022.

[8] A. Fallah, Q. Saleem, and B. Koc, "Assessment of mechanical properties and shape memory behavior of 4d printed continuous fiber-reinforced petg composites," *Composites Part A: Applied Science and Manufacturing*, vol. 181, p. 108165, 2024.

[9] A. Ibrahim, A. Klopocinska, K. Horvat, and Z. A. Hamid, "Graphene-based nanocomposites: Synthesis, mechanical properties, and characterizations," *Polymers*, vol. 13, no. 17, p. 2869, 2021.

[10] I. M. Alarifi, "Mechanical properties and numerical simulation of fdm 3d printed petg/carbon composite unit structures," *Journal of Materials Research and Technology*, vol. 23, pp. 656–669, 2023.

[11] P. Ramachandran, P. Pandian, V. Ramamoorthi, and J. J. B. John, "Influence of process parameters on the mechanical properties of carbon fibre reinforced petg," *Mechanics of Advanced Composite Structures*, vol. 13, no. 1, pp. 171–184, 2026.

[12] A. Özen, B. E. Abali, C. Völlmecke, J. Gerstel, and D. Auhl, "Exploring the role of manufacturing parameters on microstructure and mechanical properties in fused deposition modeling (fdm) using petg," *Applied Composite Materials*, vol. 28, no. 6, pp. 1799–1828, 2021.

[13] T. K. Gupta, N. Mounika, A. Saxena, N. K. Maurya, M. Jagga, and G. Sood, "Influence of raster angle on mechanical properties for fdm 3d-printed pla polymer," *Green Materials*, pp. 1–10, 2025.

[14] V. Chaudhary, C. Ahlawat, B. Sharma, R. Sahu, and N. K. Maurya, "Biodegradation and characterization of 3-d printed pla-based polymer composites reinforced with cellulose-based hemp/kenaf fibers and coconut/walnut fillers," *Polymer Composites*, 2025.

[15] N. K. Maurya, V. Rastogi, and P. Singh, "An overview of mechanical properties and form error for rapid prototyping," *CIRP Journal of Manufacturing Science and Technology*, vol. 29, pp. 53–70, 2020.

[16] S. Raja, M. Jayalakshmi, M. A. Rusho, V. K. Selvaraj, J. Subramanian, S. Yishak, and T. A. Kumar, "Fused deposition modeling process parameter optimization on the development of graphene enhanced polyethylene terephthalate glycol," *Scientific Reports*, vol. 14, no. 1, p. 30744, 2024.

[17] B. Malekmohammadi, B. Zahraie, and R. Kerachian, "Ranking solutions of multi-objective reservoir operation optimization models using multi-criteria decision analysis," *Expert Systems with Applications*, vol. 38, no. 6, pp. 7851–7863, 2011.

[18] S. K. Sahu, P. R. Sreekanth, K. K. Saxena, and Q. Ma, "Effect of graphene reinforcement on the tensile and flexural properties of thermoplastic polyurethane nanocomposite using experimental and simulation approach," *Advances in Materials and Processing Technologies*, pp. 1–17, 2024.

[19] T. Marchment, J. Sanjayan, and M. Xia, "Method of enhancing interlayer bond strength in construction scale 3d printing with mortar by effective bond area amplification," *Materials & Design*, vol. 169, p. 107684, 2019.